08

Formation of inhomogeneous oxide and suboxide layers on an ultra-thin metal film by multiple oxidation and ion sputtering

© A.V. Lubenchenko,[1] D.A. Ivanov,[1] O.I. Lubenchenko,[1] A.B. Pavolotsky,[2] D.S. Lukiantsev,[1] V.A. Iachuk,[1] O.N. Pavlov[1]

[1] National Research University „MPEI“,
111250 Moscow, Russia
[2] Chalmers University of Technology,
41296 Göteborg, Sweden
e-mail: LubenchenkoAV@mpei.ru

Received March 30, 2022
Revised March 30, 2022
Accepted March 30, 2022

A technique of controlled formation of multilayer oxide and suboxide layers on a thin metal film. An opportunity of controlled generation of films containing an ultra-thin suboxide layer inside a higher oxide layer and films being a periodic layered structure with alternating oxide layers of various oxidation levels. A structure containing alternating ultra-thin layers of higher oxide and suboxide layers on a niobium film.

Keywords: metal-oxide films, controlled film formation, layer chemical and phase profiling, X-ray photoelectron spectroscopy.

DOI: 10.21883/TP.2022.08.54561.68-22

Introduction

Ultrathin metal oxide films find their application in the creation of memristors [1,2], which, in turn, are a key element of non-volatile resistive random access memory (RRAM) [3,4]. For memristors based on ultrathin metal-oxide films, it is necessary to form oxygen-depleted layers (suboxide layers) and/or layers with oxygen vacancies. The functional parameters of the memristor as RRAM elements (the number of write/read cycles, write and erase voltages, etc.) depend on the layered chemical and phase composition and thickness of the active layer.

Memristive switching is observed in various materials and structural devices. Thus, systems consisting of metal–oxide–metal based on niobium oxides have attracted special attention by the simplicity of their structure, reliability and variety of switching characteristics, which depend on the layer-by-layer stoichiometry of the ultrathin film, electrode material, device geometry and operating conditions [5].

Resistive switching of the metal–oxide–metal system is explained by such phenomena as the migration of oxygen ions and the formation of oxygen vacancies under the action of an electric field or flowing current. There are various ways to produce metal suboxides for memristive structures. In the study [6], the authors manufactured a device with improved memristive characteristics based on $Ti/TiO_x/Ti/Ti/TiO_x/Ti$ and $Ti/TiO_x/Ti$ by magnetron sputtering in pulsed mode with By the subsequent controlled injection of oxygen into the chamber, X-ray diffraction analysis was performed and the crystal phases were determined. However, this paper does not present the results of the layered phase composition of targets, which, in our opinion, affects the characteristics of memristive structures. The authors of [7] demonstrate the possibility of creating a nanosuboxide layer from a layer Ta_2O_5 previously sputtered by atomic layer deposition using ion beam spraying Ar^+, but they failed to identify the phases TaO_x and perform a layered phase analysis of the targets. Thus, the production of transitional suboxide layers of a certain composition, determined by the proper operation of the memristive device, is possible with constant monitoring of phases during their formation, i.e. it is necessary to conduct a quantitative layered phase chemical analysis of the surface.

In this paper, we propose a multi-stage technology for the formation of multilayer oxide and oxide layers on an ultrathin metal film in several stages: 1) sputtering of a homogeneous ultrathin metal film onto a substrate in a vacuum chamber by magnetron sputtering with control of the thickness of the sprayed film; 2) atmospheric oxidation of the film after unloading from the chamber; 3) loading into a vacuum chamber; 4) determination of the layered chemical and phase composition of the oxidized metal film; 5) spraying of the oxide layer with sliding ion beams in order to reducing its thickness, while monitoring the *in situ* layer-by-layer chemical and phase composition of the film; 6) modification of the oxide layer into a suboxide layer (a layer with a depleted oxygen content) due to the predominant atomization of oxygen by low-current ion beams with control of the layer-by-layer chemical and phase composition of the film; 7) controlled oxidation in the airlock chamber, forming a layer of higher oxide on the upper surface; 8) determination of the layer-by-layer chemical and the phase composition of the oxidized metal film. This approach will allow the formation of oxide and

sub-oxide layers with certain thicknesses and composition on a thin metal film.

In this paper, the formation of a multilayer oxide and suboxide structure on thin niobium films is demonstrated.

1. Experiment

Niobium films were deposited on a silicon substrate by magnetron sputtering in the Pfeiffer Vacuum SLS630G installation. The film thickness during sputtering was controlled by the known sputtering rate (the sputtering rate was confirmed during the examination of films by transmission electron microscopy (TEM)). Films with a thickness of 50 and 15 nm on a silicon substrate were used. To form a thick layer of higher oxide, the films were exposed to air for several hours. Spraying and modification of the film were carried out by directed ion beams Ar^+ under vacuum conditions using an ion cannon SPECS Ion Source IQE 12/38 (when spraying: ion energy — 1 keV, angle of incidence — 70° to normal, ion current — 1.5 μA; when modified: ion energy — 0.5 keV, angle of incidence — 70° to normal, ion current — 0.5 μA). Controlled oxidation in the airlock chamber, forming a layer of higher oxide on the upper surface, was carried out in two modes: short-term oxidation in the atmosphere for 1 min, long-term oxidation in the atmosphere for 15 min.

X-ray photoelectron spectra were obtained using the electron-ion spectroscopy module based on the Nanofab 25 (NT-MDT) platform. An ultra-high oil-free vacuum of the order of 10^{-6} Pa was achieved in the analytical chamber. The spectra were taken with an electrostatic hemispherical energy analyzer SPECS Phoibos 225 using an X-ray gun with an Mg anode. Calibration of the energy analyzer was performed using samples from Cu, Ag and Au. The energy resolution of the spectrometer along the $Ag3d_{5/2}$ line was 0.78 eV (full width at half height) for non-monochromatic X-ray radiation MgK_α. The energy analyzer worked in the FAT mode (Fixed Analyzer Transmission). For survey spectra, the deceleration energy in the lens of the energy analyzer was set to $E_{pass} = 80$ eV, for detailed — $E_{pass} = 20$ eV.

2. Layered chemical and phase analysis

One of the non-destructive methods of analyzing ultrathin films is X-ray photoelectron spectroscopy (XPS). Chemical and phase analysis of the surface is carried out with the help of the XPS. In the standard XPS method, relative concentrations are calculated under the assumption of uniformity of the target over the entire depth of analysis.

Real surfaces are always heterogeneous and multicomponent in depth. Failure to take this into account leads to significant errors and devalues the very information about the relative concentrations of elements.

In this paper, for the layered chemical and phase composition of multicomponent multilayer films, we used the method [8,9]. It consists of: a new method for subtracting the background of repeatedly inelastic scattered photoelectrons, taking into account the heterogeneity of inelastic scattering in depth; a new method for decomposing a photoelectronic line into component peaks, taking into account the physical nature of various decomposition parameters; solving the problem of subtracting the background and decomposing a photoelectronic line together; determining the thicknesses of layers of a multilayer target using a simple formula.

Calculation of the thickness of a multilayer target is carried out according to the formula [8]:

$$d_i = \lambda_{Io} \cos\theta \ln\left(\frac{I_i/(n_i\omega(\gamma)\lambda_i)}{\sum_{j=0}^{i-1} I_j/(n_j\omega(\gamma)\lambda_j)} + 1\right), \qquad (1)$$

where d_i — thickness of the ith layer, n — atomic concentration, $\omega(\gamma)$ — differential cross section of the photoelectron birth [10], γ — the angle between the direction of incident radiation and the direction to the energy analyzer, λ — the average free inelastic path length (IMFP) (IMFP was calculated using the formula TPP2M [11]), θ — the angle between the direction to the energy analyzer and the normal line to surfaces, I_i — intensity of the ith peak. The numbering of the layers will be carried out from the substrate from the bottom up.

Depth sensitivity and depth of sensing can be estimated by the formula (1). Consider a homogeneous layer of niobium oxide Nb_2O_5 on a niobium substrate. Since we determine the partial intensities using our method with an accuracy of 1%, we can determine the ratio of the partial intensities of the peaks of photoelectrons from the upper layer and the substrate $I_{Nb2O5}/I_{Nb} = 1/100$. Then from the formula (1) we get $d_{\min} = 0.1$ nm. The depth of probing is determined by putting $I_{Nb2O5}/I_{Nb} = 100/1$. By the formula (1) we get $d_{\max} = 13.9$ nm.

The procedure of determining the layered profile is based on the following target model. The target consists of several flat layers on a substrate. Each layer is homogeneous and can be multicomponent. This situation is justified, since in the XPS, the signal is taken from an area whose characteristic dimensions are orders of magnitude larger than the depth of sounding, and the signal will be averaged over the measurement area. Heterogeneities (islands, interlayer roughness, inclusions, etc.) are averaged over the layer. The degree of heterogeneity will characterize the relative concentrations of a particular phase of the elements and the thickness of the layer. The relative concentrations of bound elements in the layer are calculated from the intensities of the spectral lines of bound elements determined after the decomposition procedure of the photoelectronic line into component peaks. The sequence of different layers in the accepted target model follows from knowledge of the history of creation and subsequent „life “ target. The studied ultrathin films were deposited in a vacuum chamber on silicon substrates. After unloading from the chamber, the surface is oxidized with the formation of oxide and

oxide layers on top. Since oxidation occurs from the surface, the degree of oxidation decreases deep into the target. In addition, hydrocarbon layers will be deposited on top of the layers.

When ions are sprayed on the surface of an oxidized metal film, oxygen is primarily sprayed from the near-surface region. For example, when spraying with argon ions with an energy of 1 keV, falling at an angle of 70° from the normal, on an oxide film Nb_2O_5 with a thickness of 8 nm on a niobium substrate, the coefficient atomization for niobium is 0.8 atom/ion, and for oxygen — 4.9 atom/ion; the average ion penetration depth is 1.9 nm. When the ion energy changes to 500 eV, the atomization coefficient for niobium becomes 0.4 atom/ion, and for oxygen — 3.0 atom/ion, the average ion penetration depth is 1.3 nm. The data were obtained by the Monte Carlo method using the TRIM [12] program. Thus, when spraying, we can form oxygen-depleted layers. By changing the energy and angle of incidence of ions, it is possible to create layers with different phase composition and thickness.

X-ray photoelectron spectra can be used to analyze the chemical bonds of elements and the chemical composition of a substance. To do this, the X-ray photoelectronic line of a certain element is decomposed into corresponding peaks. The structure of an X-ray photoelectronic line can be quite complex due to the superposition of peaks from various chemically bound elements (elements in different phase states), satellite peaks, etc. In addition, the shape and width of the peaks depend on various factors, and these peaks overlap. To decompose the X-ray photoelectronic line, we used the procedure described in [9]:

1) The profile of a complex photoelectronic spectral line formed by photoelectrons from a chemically unrelated element and elements in various chemically bound states is determined by the formula

$$LS(E) = I_0 LS_2(E) + \sum_{j=1}^{J} I_j LS_2(E - \Delta E_{CS_j}), \qquad (2)$$

where ΔE_{CS_j} — the chemical shift energy of the jth element, J — the number of chemically bonded elements, I_j — the intensity of the spectral line of the jth a chemically bound element.

2) Due to the spin-orbit interaction, a doublet structure will be observed in the XPS spectra for lines formed by photoelectrons with p-, d-shells. The profile of spin-orbital doublets is described by the formula

$$LS_2(E) = (LS_1(E) + \alpha LS_1(E - \Delta E_{SO}))/(1 + \alpha), \qquad (3)$$

where α — the ratio of the intensities of the spin-orbital splitting lines of the photoelectronic level (for p-shell $\alpha = 1/2$, for d-shell $a = 2/3$), ΔE_{SO} — the energy of the spin-orbital interaction.

3) To account for the non-monochromacy of the X-ray gun, the expression is used

$$LD_1(E) = P(E) + \sum_{k=1}^{K} I_{sattelitek} P(E + \Delta E_{sattelitek}), \qquad (4)$$

where $I_{satellitek}$ and $\Delta_{satellitek}$ are the relative intensities and energy shifts of the satellites, these parameters depend on the anode material of the X-ray gun.

4) The shape of the partial spectral line $P(E)$ of photoelectrons with kinetic energy E is determined by the convolution of functions describing the natural shape of the line and the instrument broadening. The natural shape of the line is described by the expression Donyah–Sunzhicha [13] $D(E, \delta, \alpha_{DS})$ (here δ — natural width of the electronic level, α_{DS} — Anderson singularity index; at $\alpha_{DS} = 0$ the expression of Donyah–Sunzhich passes into the Lorentz function), and the instrument broadening function $G(E, W)$ — by the Gaussian function (here $W = \sqrt{W_{sp}^2 + W_{h\nu}^2}$, $W_{h\nu}$, W_{sp} — width of the X-ray line and instrument broadening).

For chemically pure elements, the intrinsic width δ, the coefficient α_{DS}, the binding energy BE_0 and the spin-orbit interaction energy ΔE_{SO} are determined by experimental data from the Handbook of X-ray Photoelectron Spectroscopy [14]. The chemical shift energy is almost linearly proportional to the degree of oxidation, so it is sufficient to determine the chemical shift energy for the maximally oxidized element. For niobium pentoxide, we used the value $\Delta E_{CSNb2O5} = 5.3$ eV (line Nb $3d$) [15]. Since the spectra were taken at the same settings, the same values were used for all calculations: $W_{h\nu} = 0.68$ eV, $W_{sp} = 0.72$ eV.

When decomposing a photoelectronic line into components, the intensity peaks of the spectral lines of chemically bound elements are found using fitting algorithms (for example, the Levenberg-Marquardt algorithm).

Fig. 1 shows the results of decomposition of the spectral line Nb $3d$ into various phase components for targets with films after the research stage: after sputtering (20 min) (*a*); after short-term oxidation (1 min) (*b*). Experimental data are indicated by circles, a solid line — theoretical interpretation of the spectrum, shaded areas — partial theoretical spectra.

The spectral photoelectronic line Nb $3d$ after each stage will consist of a different set of doublet lines. In each doublet line, the ratio of the areas of two spin-orbital peaks will correspond to 2:3 (see the formula (2)). The total spectral line may consist of 6 doublets corresponding to pure niobium and the phase states of niobium oxide: Nb, Nb_2O, NbO, Nb_2O_3, NbO_2, Nb_2O_5.

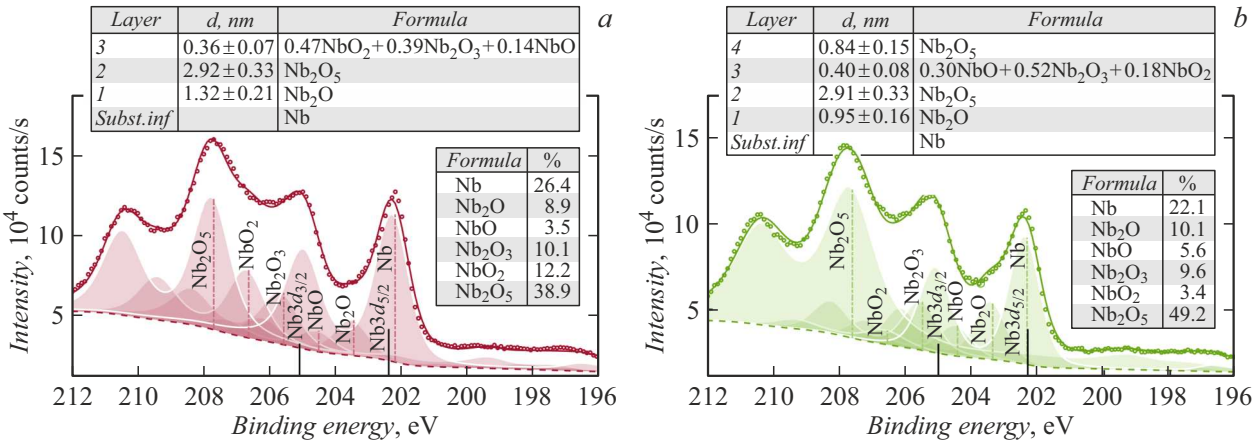

Figure 1. X-ray photoelectronic spectra: spectral line Nb3*d*.

3. Formation of heterogeneous multilayer oxide and oxide layers

3.1. Formation of an ultrathin suboxide layer inside a layer of higher oxide

The experiments were carried out with a 50 nm thick niobium film oxidized in air on a silicon substrate. To form a suboxide layer inside the higher oxide layer, the following steps were carried out: a) spraying of the oxide layer with argon ion beams with an energy of 500 eV for 20 min at an angle of 70° from the normal, ion current — 1.5 μA; b) modification of the oxide layer by ion beams with an energy of 500 eV for 10 min at an angle of 70° from the normal, ion current — 0.5 μA; c) controlled oxidation in the lock chamber for 1 min; d) controlled oxidation in the airlock chamber for 15 min. Two oxidation stages were chosen to demonstrate the growth rate of the higher oxide on the film surface depending on the oxidation time.

Fig. 2 shows the X-ray photoelectron spectra taken after each stage: survey spectra (*a*); spectral line Nb 3d (*b*). The spectra are indicated by numbers: *1* — before spraying; *2* — after spraying (20 min); *3* — after modification (10 min); *4* — after short-term oxidation (1 min); *5* — after long-term oxidation (15 min).

Fig. 2, *b* shows the dynamics of changes in spectral lines Nb 3*d* after various stages of film formation. If before sputtering, the spectrum is formed mainly by photoelectrons from the layer of the higher oxide Nb_2O_5, then after sputtering, the doublet spectral lines of the higher oxide are superimposed on the doublet spectral lines of suboxides and pure niobium. These lines are shifted relative to the pure niobium lines by different values of the chemical shift energy depending on the degree of oxidation of niobium. The contribution of peaks of higher oxide, suboxides and pure niobium to the total intensity of the spectral line varies after each stage of the formation of an heterogeneous film.

Table 1 presents the results of layer-by-layer chemical and phase analysis after each stage of formation of oxide and suboxide layers on a niobium film with a thickness of 50 nm.

Layer-by-layer analysis shows that during atmospheric oxidation of films, a transition layer is formed under a layer of higher oxide between a higher oxide and a metal with a thickness of about 2 nm. During spraying, about 4 nm layers of the higher oxide were removed. After modification, a suboxide layer with a thickness of 1 nm was formed on the surface. After a short-term oxidation from above, almost half of the suboxide layer was oxidized to a higher oxide. After 15 min oxidation, a layer of higher oxide of the order of 2 nm was formed. Layers with thicknesses less than 0.5 nm can be interpreted not as continuous layers, but as heterogeneous layers with discontinuities, or as island structures.

3.2. Formation of alternating suboxide layers with varying degrees of metal oxidation

The experiments were carried out with a 15 nm thick niobium film oxidized in air on a silicon substrate. To form alternating suboxide and oxide layers, the following steps were carried out: a) sputtering of the oxide layer with argon ion beams with an energy of 1 keV for 30 min at an angle of 70° to the normal, ion current — 1.5 μA; b) modification of the oxide layer by ion beams with an energy of 500 eV for 15 min at an angle of 70° to the normal, ion current — 0.5 μA; c) controlled oxidation in the lock chamber for 1 min; d) modification of the oxide layer by ion beams with an energy of 500 eV for 15 min at an angle of 70° from the normal, ion current — 0.5 μA.

Fig. 3 shows the X-ray photoelectron spectra (spectral line Nb 3*d*) taken after each stage. The spectra are indicated by numbers: *1* — before spraying; *2* — after spraying (30 min); *3* — after modification (15 min); *4* — after short-term oxidation (1 min); *5* — after modification (15 min).

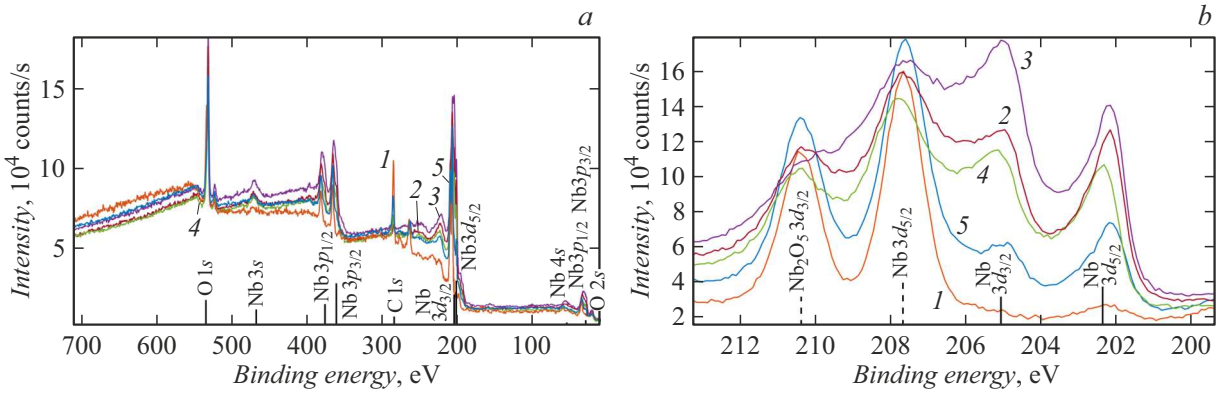

Figure 2. X-ray photoelectronic spectra: *a* — overview spectrum; *b* — spectral line Nb3*d*.

Table 1. Layered chemical and phase composition of heterogeneous multilayer films

Layers	1		2		3		4		5	
	d, nm	Formula	*d*, nm	Formula	*d*, nm	Formula	*d*, nm	Formula	*d*, nm	Formula
4	–	–	–	–	–	–	0.84 ± 0.15	Nb_2O_5	1.58 ± 0.23	Nb_2O_5
3	–	–	0.36 ± 0.10	0.47 NbO_2+ 0.39 Nb_2O_3+ 0.14 NbO	1.02 ± 0.17	0.32 NbO_2+ 0.42 Nb_2O_3+ 0.26 NbO	0.40 ± 0.08	0.30 NbO_2+ 0.52 Nb_2O_3+ 0.18 NbO	0.19 ± 0.04	0.66 NbO_2+ 0.18 Nb_2O_3+ 0.16 NbO
2	7.5 ± 0.4	Nb_2O_5	2.9 ± 0.3	Nb_2O_5	2.5 ± 0.3	Nb_2O_5	2.5 ± 0.3	Nb_2O_5	2.5 ± 0.3	Nb_2O_5
1	2.1 ± 0.3	Nb_2O	1.3 ± 0.3	Nb_2O	1.2 ± 0.3	Nb_2O	1.0 ± 0.3	Nb_2O	1.0 ± 0.3	Nb_2O
0		Nb		Nb		Nb		Nb		Nb

Note. Column numbers: 1 — before spraying; 2 — after spraying (20 min); 3 — after modification (10 min); 4 — after short-term oxidation (1 min); 5 — after long-term oxidation (15 min).

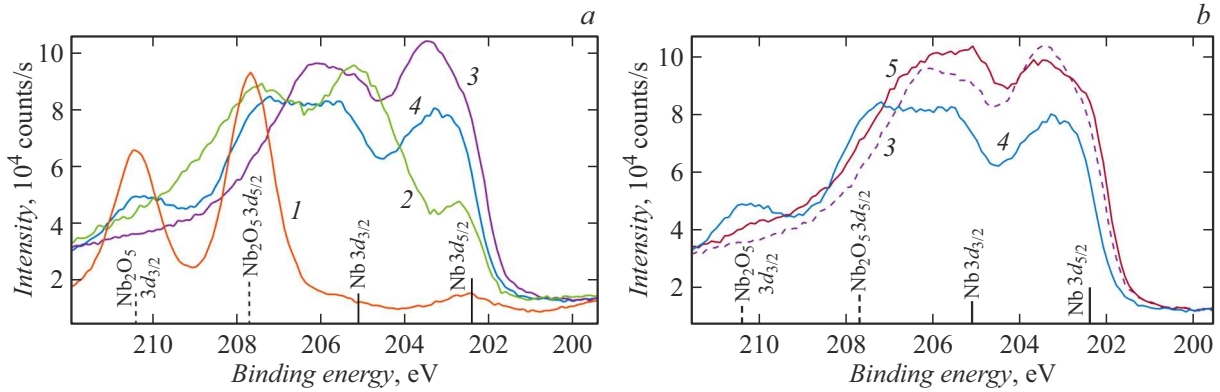

Figure 3. X-ray photoelectronic spectra: spectral line Nb3*d*.

Table 2 presents the results of layer-by-layer chemical and phase analysis after each stage of formation of oxide and suboxide layers on a niobium film with a thickness of 15 nm.

Layer-by-layer analysis shows that during atmospheric oxidation of films, a transition layer is formed under a layer of higher oxide between a higher oxide and a metal with a thickness of about 2 nm. During spraying, about 6 nm layers of higher oxide were removed. Spraying with ions with an energy of 1 keV leads to the formation of a suboxide layer of greater thickness on top than when spraying with ions of 500 eV. This is explained by the fact that the average penetration depth of ions with an energy of 1 keV is one and a half times greater than for ions with an energy of 0.5 keV. After the first modification, a suboxide layer with a thickness of about 2 nm was formed on the surface. Short-term oxidation leads to the formation of a monolayer of

Table 2. Layered chemical and phase composition of heterogeneous multilayer films

Layers	1		2		3		4		5	
	d, nm	Formula	*d*, nm	Formula	*d*, nm	Formula	*d*, nm	Formula	*d*, nm	Formula
4	–	–	–	–	1.62 ± 0.23	0.22 NbO+ 0.78 Nb_2O	0.65 ± 0.10	Nb_2O_5	0.96 ± 0.16	Nb_2O
3	–	–	1.43 ± 0.21	0.16 NbO_2+ 0.34 Nb_2O_3+ 0.50 NbO	0.33 ± 0.06	0.67 NbO_2+ 0.33 ± 0.06	1.33 ± 0.11	0.27 NbO_2+ 0.36 NbO+ 0.37 Nb_2O	0.88 ± 0.15	0.24 NbO_2+ 0.21 Nb_2O_3+ 0.55 NbO
2	8.4 ± 0.4	Nb_2O_5	2.3 ± 0.3	Nb_2O_5	1.0 ± 0.2	Nb_2O_5	0.8 ± 0.3	Nb_2O_5	1.1 ± 0.3	Nb_2O_5
1	1.6 ± 0.3	Nb_2O	1.4 ± 0.3	Nb_2O	1.3 ± 0.3	Nb_2O	1.0 ± 0.3	Nb_2O	0.9 ± 0.3	Nb_2O
0		Nb		Nb		Nb		Nb		Nb

Note. Column numbers: 1 — before spraying; 2 — after spraying (30 min); 3 — after modification (15 min); 4 — after short-term oxidation (1 min); 5 — after modification (15 min).

higher oxide. The second modification creates a layer with a low degree of niobium oxidation on top. With increasing depth, the degree of oxidation of niobium increases and at a depth of 2 nm becomes maximum. After 3 nm, a layer with a low degree of oxidation is observed. This layer has been preserved from the original structure before spraying.

Conclusion

This paper proposes a technology for the formation of multilayer oxide and oxide layers on an ultrathin metal film in several stages of ion sputtering, modification and oxidation. After each stage, the *in situ* control of the layer composition of the film is carried out. The applied procedure of analyzing the layered composition of films [9] allows, without destroying, to determine the layered chemical and phase composition of multilayer multicomponent films on various substrates with subnanometer accuracy to a depth of about ten nanometers. By combining the parameters of ion sputtering (angle of incidence on the target, ion energy, ion current, sputtering time), the order and time of oxidation, it is possible to achieve the formation of a variety of metal-suboxide structures. Reliable knowledge of the layered chemical and phase composition of multilayer multicomponent films and its changes depending on various external factors will improve the technology of obtaining such films and predict the behavior of these films at various points of operation.

Conflict of interest

The authors declare that they have no conflict of interest.

References

[1] L. Chua. IEEE Tr. Circuit Theor., **18**, 507–519 (1971).
[2] A.N. Belov, A.A. Perevalov, V.I. Shevyakov. Izv. vuzov. Fizika i Tekhnologiya, **22**, 42017305 (2017). (in Russian)
[3] A. Belov, D. Korolev, I. Antonov, V. Kotomina, A. Kotina, E. Gryaznov, A. Sharapov, M. Koryazhkina, R. Kryukov, S. Zubkov, A. Sushkov, D. Pavlov, S. Tikhov, O. Morozov, D. Tetelbaum. Adv. Mater. Technol., **5**, 1900607 (2020). DOI: 10.1002/admt.201900607
[4] A. Gudkov, A. Gogin, M. Kick, A. Kozlov, A. Samus. Elektronika: Nauka, Tekhnologiya, Biznes, 156–162 (2014). (in Russian)
[5] S.K. Nath, S.K. Nandi, S. Li, R.G. Elliman. Nanotechnology, **31**, 235701 (2020).
[6] M. Gul, H. Efeoglu. J. Mater. Sci. Mater. El., **33**, 7423–7434 (2022). DOI: 10.1007/s10854-022-07864-z
[7] W.D. Songa, J.F. Yinga, W. He, V.Y.-Q. Zhuo, R. Ji, H.Q. Xie, S.K. Ng, Serene L.G. Ng, Y. Jiang. Appl. Phys. Lett., **106**, 031602 (2015). doi.org/10.1063/1.4906395
[8] A.V. Lubenchenko, A.A. Batrakov, I.V. Shurkaeva, A.B. Pavolotsky, S. Krause, D.A. Ivanov, O.I. Lubenchenko. J. Surf. Invest. X-Ray, **12**, 692–700 (2018).
[9] A.V. Lubenchenko, A.A. Batrakov, A.B. Pavolotsky, O.I. Lubenchenko, D.A. Ivanov. Appl. Surf. Sci., **427**, 711–721 (2018).
[10] J.J. Yeh, I. Lindau. Atom. Data Nucl. Data, **32**, 1 (1985).
[11] S. Tanuma, C.J. Powell, D.R. Penn. Surf. Interface Anal., **21.3**, 165 (1994).
[12] J.P. Biersack, L.G. Haggmark. Nucl. Instrum. Meth., **174**, 257–269 (1980).
[13] S. Doniach, M. Sunjic. J. Phys. C Solid State., **3.2**, 285 (1970).
[14] J.F. Moulder, W.F. Stickle, P.E. Sobol, K.D. Bomben. *Handbook of X Ray Photoelectron Spectroscopy: A Reference Book of Standard Spectra for Identification and Interpretation of XPS Data* (Physical Electronics, 1979)
[15] A.V. Naumkin, A. Kraut-Vass, C.J. Powell. *NIST X-ray photoelectron spectroscopy database* (2008)